



# Nanostructured Cobalt Zinc Ferrite Thin Films For Gas Sensor Application

Vaishali S. Dhoble<sup>a</sup> Avinash R. Gaikwad<sup>b</sup> and Sadeep A. Kardile<sup>c</sup>

<sup>a</sup> Department of physics, D. K. A. S. C. sCollege , ICH, Kolhapur

<sup>b</sup> Department of Physics, Yeshwant Mahavidyalaya, Nanded, MS India – 431 602,

## Abstract:

*In this work, porous thin films were obtained from a Co<sub>1</sub>Zn<sub>0.65</sub>Fe<sub>1.35</sub>O<sub>4</sub> target sputtered under pure argon plasma, by optimizing the deposition parameters (gas pressure, power). The deposition time was adjusted in order to obtain an average thickness of 300 nm. Ferrite compounds are very important because of their optical, electrical or magnetic properties. Moreover, many papers relate to their development as possible gas sensor. In this study, we were interested in using cobalt–Zinc–ferrite as sensitive layer for CO<sub>2</sub> sensor devices. Such an application required a high surface activity, and consequently a small crystallite size and a large surface area. The physical vapor deposition (RF-sputtering) is widely used for thin film synthesis.*

**Keywords:** Thin film; Ferrite; Sputtering; Gas sensor; Surface measurement; Nanostructured

## 1. Introduction

Structural (G-XRD) and microstructural (SEM-FEG, gas adsorption, electron microprobe) analyses were carried out on these thin films. The chemical composition was found to be homogeneous on the whole surface of the samples. The grain size ranged from 10 to 25 nm. The surface enhancement factor (SEF) was about 100 m<sup>2</sup>/m<sup>2</sup>, which is equivalent to a specific surface area of 76 m<sup>2</sup>/g for the ferrite layer. In conclusion, these nanostructured cobalt–Zinc–ferrite films appear to be quite suitable for an application as gas sensors.

Many work on various materials as gas sensors were published in recent years. Semiconductor gas sensors like SnO<sub>2</sub>, MnO or Fe<sub>2</sub>O<sub>3</sub> have been well studied to detect most of the reducing gases and they are considered interesting for their low cost and simple sensing method [1], [2], [3], [4], [5], [6] and [7]. Nevertheless, there still exist some problems with them, for example, the poor selectivity of SnO<sub>2</sub> [8] or the high working temperature of MnO (400–450 °C) [9]. In order to optimize the performance of these sensors, many other studies were focused on the use of noble metal catalysts, such as Ag, Pt and Pd [10], materials doping [11] or mixed-oxide systems such as SnO<sub>2</sub>–WO<sub>3</sub>, TiO<sub>2</sub>–WO<sub>3</sub>, SnO<sub>2</sub>–TiO<sub>2</sub> [12]. Several new materials are also being tested. Transition metal ferrites are a family of oxides that play an important role in a wide variety of fields because of the variety of transition metal cations that can be incorporated into the

lattice of the parent magnetite ( $\text{Fe}_2^+ \text{Fe}_2^{3+}\text{O}_4^{2-}$ ) structure. In the case where these ferrites are used for catalytic [13] and [14], magnetic or electrical applications [15], they are prepared in the form of ceramics materials with very high density.

On the contrary, in applications for gas sensor devices, lower density and higher surface area are required. With this intention, several methods of preparation of these compounds are known. Co-precipitation [16], [17] and [18], microemulsion [19], pulsed wire discharge [20], citrate [17] or hydrothermal [21] processes are employed in order to obtain nanometer-sized powders. Spray pyrolysis [22], ultrasound-enhanced ferrite plating [23], plasma spray [24], or sputtering [25] and [26] depositions can be used to make ferrite planar devices. That is precisely this last method that was used for our study.

This paper relates on the preparation of porous thin films obtained from a  $\text{Co}_1\text{Zn}_{0.65}\text{Fe}_{1.35}\text{O}_4$  target sputtered under pure argon plasma and their characterization for an application as gas sensors.

## 2. Experimental

### 2.1. Film deposition

Cobalt–Zinc–ferrite thin films were worked out by RF-sputtering method using a  $\text{Co}_1\text{Zn}_{0.65}\text{Fe}_{1.35}\text{O}_4$  ceramic target. The apparatus is an Alcatel SCM 400 equipped with a RF generator (13.56 MHz), a pumping system (a mechanical pump coupled with a turbo molecular pump) which allows reaching a residual pressure down to  $1 \times 10^{-5}$  Pa, a gas flow controller, a cooled target holder, a removable magnet placed behind the target when the magnetron configuration is used, and four cooled sample holders. The target was produced starting from commercial oxides mixture with 99.999% in purity. The films were deposited on glass slides for all studies. A residual vacuum of  $5 \times 10^{-5}$  Pa was reached in the sputtering chamber before introducing the deposition gas (argon). The distance between the target and the substrates was 90 mm. In order to obtain two clearly different kinds of microstructure, two gas pressures were used for this study, 2 and 0.5 Pa. In both cases a pre-sputtering process (20 min) was made in order to prevent the incorporation of impurities in the films. At high pressure deposits were carried out with magnetron configuration (argon flow = 55  $\text{cm}^3/\text{min}$ ) while at low pressure without magnetron configuration (argon flow = 11  $\text{cm}^3/\text{min}$ ). In these conditions, the deposition rates were 3.5 and 2.4  $\text{nm}/\text{min}$ , respectively. The conditions of deposition are summarized in Table 1. The composition of the target and thin films was determined by a Cameca SX50 electron microprobe. For each sample, ten different points were probed. The average result as well as the accuracy obtained for each analysis are summarized in the Table 2. Assuming a pure and stoichiometric spinel, the target and thin films have the following composition:  $\text{Co}_1\text{Zn}_{0.65}\text{Fe}_{1.35}\text{O}_4$

**Table 1. Sputtering deposit parameters**

<b>Target : Co<sub>1</sub>Zn<sub>0.65</sub>Fe<sub>1.35</sub>O<sub>4</sub></b>	<b>Magnetron configuration</b>	<b>Without magnetron</b>
<b>RF power (W)</b>	<b>50</b>	<b>200</b>
<b>Gas pressure (Pa)</b>	<b>2</b>	<b>0.5</b>
<b>Argon flow (cm<sup>3</sup>/min)</b>	<b>55</b>	<b>11</b>
<b>Deposition rate (nm/min)</b>	<b>3.5</b>	<b>2.4</b>
<b>Target-substrate distance (mm)</b>	<b>90</b>	
<b>Film thickness (nm)</b>	<b>300</b>	
<b>Substrate</b>	<b>Glass substrate</b>	

**Table 2. Electron microprobe analysis (atomic% of the elements)**

	<b>Target</b>	<b>Thin films</b>
<b>CO</b>	<b>14.8 ± 0.5</b>	<b>15.1 ± 0.4</b>
<b>Zn</b>	<b>8.7 ± 0.4</b>	<b>8.8 ± 0.3</b>
<b>Fe</b>	<b>19.3 ± 0.6</b>	<b>19.1 ± 0.4</b>

## 2.2. Characterizations

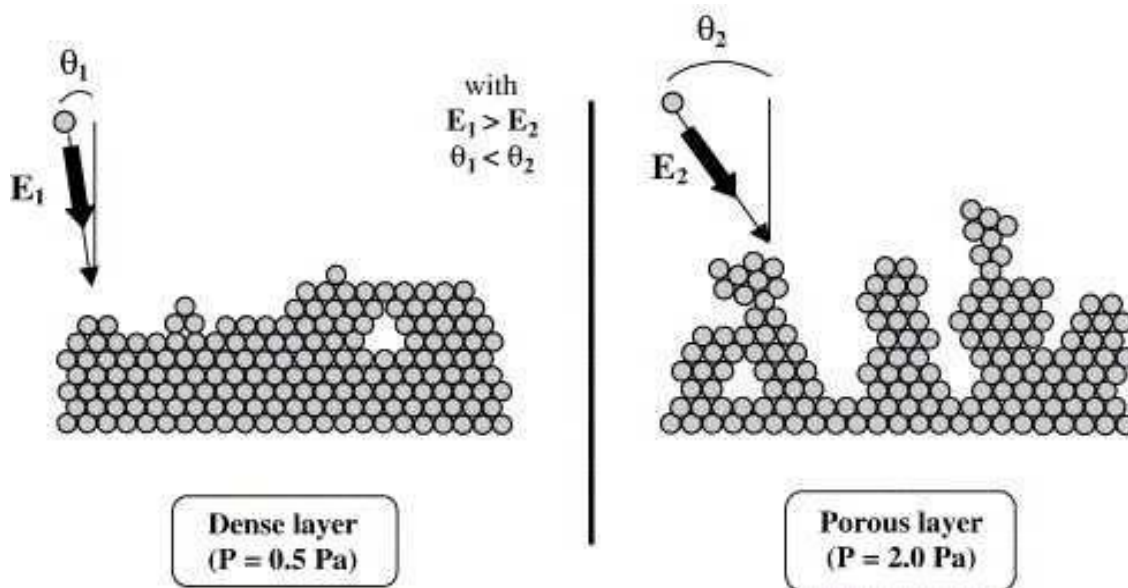
Film thicknesses were measured using a Dektak 3030ST profilometer. Structural characterizations of films and powder (target) were performed by glancing incidence XRD on a Siemens D5000 diffractometer and on a Seifert 3003  $\theta/2\theta$  diffraction unit, respectively. Morphology and microstructure of the as-deposited samples were determined by atomic force microscopy (AFM), performed on a Veeco D3000. The surface area of the films was measured using an adsorption analyser (Micromeritics ASAP 2010) operating with krypton at 77 K. Prior to measurements, the samples were heated under vacuum at different temperatures for a defined time. For each measurement, the temperature and the time of the outgassing step will be specified, when required.

## 3. Results and discussion

As we have previously explained, a sensitive layer for gas sensor application requires a high surface activity which is strongly dependent on the magnitude of their surface area and the nature of their porosity. For this study we have used RF-sputtering deposition method. Two extreme conditions of thin films preparation were used in order to compare the influence of the microstructure on the surface area. A high deposition pressure and the use of the magnetron make it possible to obtain porous layers. This can be explained by the fact that the flow of particles extracted from plasma is concentrated on a small surface (due to the presence of magnetron), which increases the number of collisions occurring in the space between the target and the substrate and causes an increase of mean incident angle ( $\theta_2$ , see Fig. 1) and thus, the appearance of shadowing effects leading to intergranular voids within the growing layer. By opposition, at low deposition pressure and without magnetron configuration, few collisions occur within the plasma; therefore incident angles tend to be close to normal ( $\theta_1$ ) and bombarding energy ( $E_1$ ) tends to be high. The

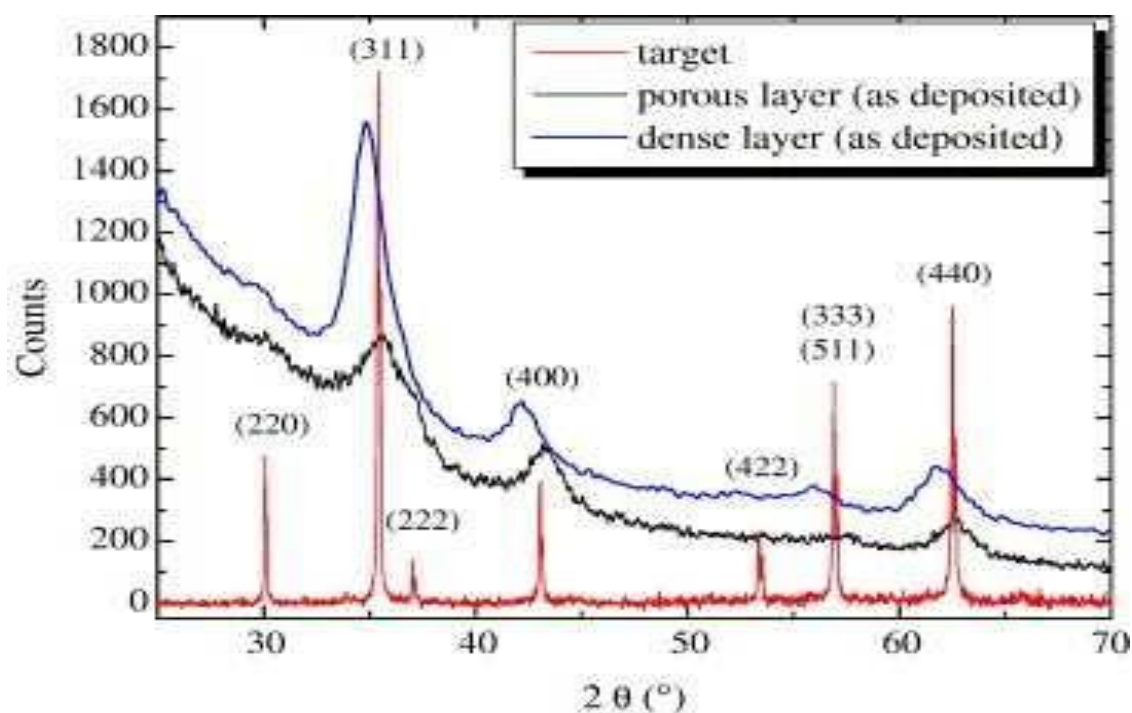
high bombarding energy leads to a high adatom mobility (atoms present at the surface of the layer) and thus, to a high film density (Fig. 1).

**Fig. 1. Schematic representation of the evolution of the microstructure according to the collision angle ( $E$  = bombarding energy,  $\theta$  = collision angle).**



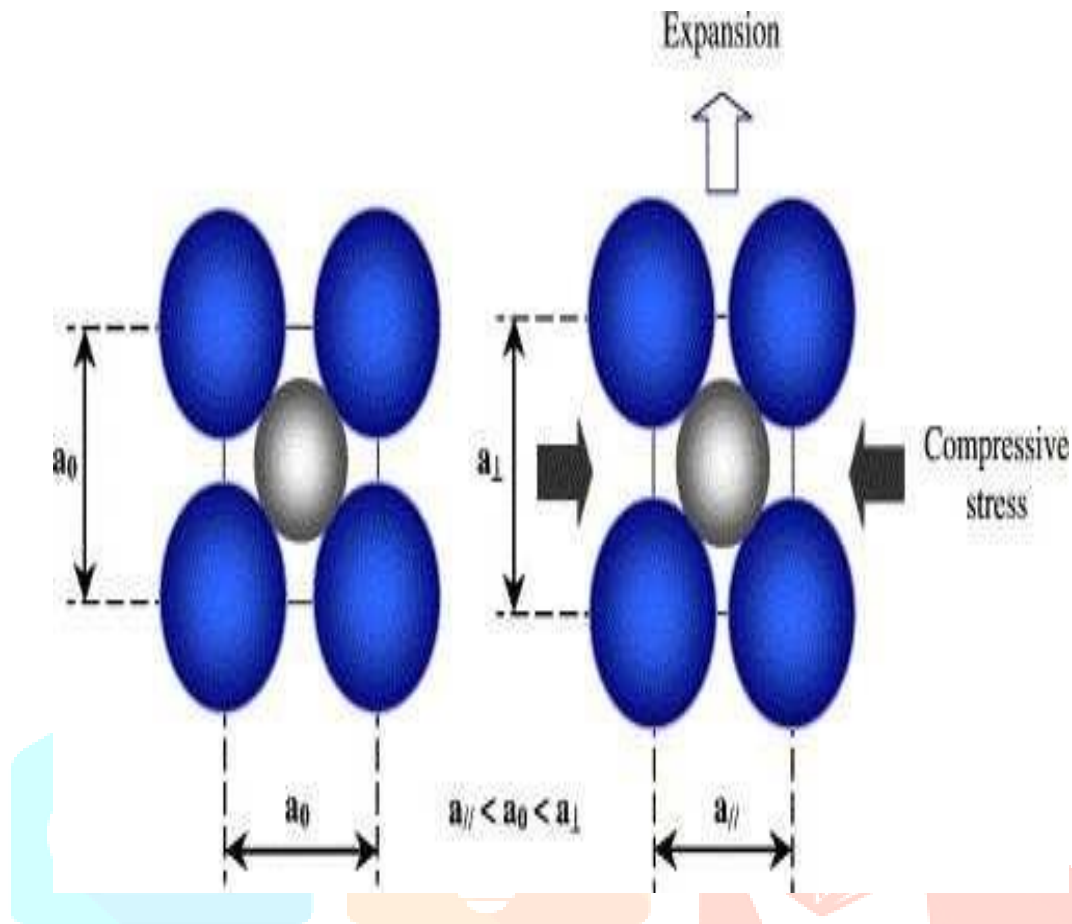
The X-ray diffraction patterns of  $\text{Co}_1\text{Zn}_{0.65}\text{Fe}_{1.35}\text{O}_4$  target and the ones of porous and dense films (300 nm thick) obtained after sputtering at 2 and 0.5 Pa, respectively, are reported in the same diagram for comparison (see Fig. 2). All the present peaks belong to the spinel structure. The width of diffraction peaks lets us suppose a weak crystallization of both porous and dense layers and therefore, the presence of nanometer-size grains. Nevertheless, diffraction peaks are better defined for the dense layer, which suppose an increase of the grain size. They are also shifted toward large inter-reticular distance, which is due to an atomic peening.

**Fig. 2. X-ray diffraction patterns for cobalt–manganese–ferrite target and thin films deposited at 2 Pa (porous layer) and 0.5 Pa (dense layer) pressure.**



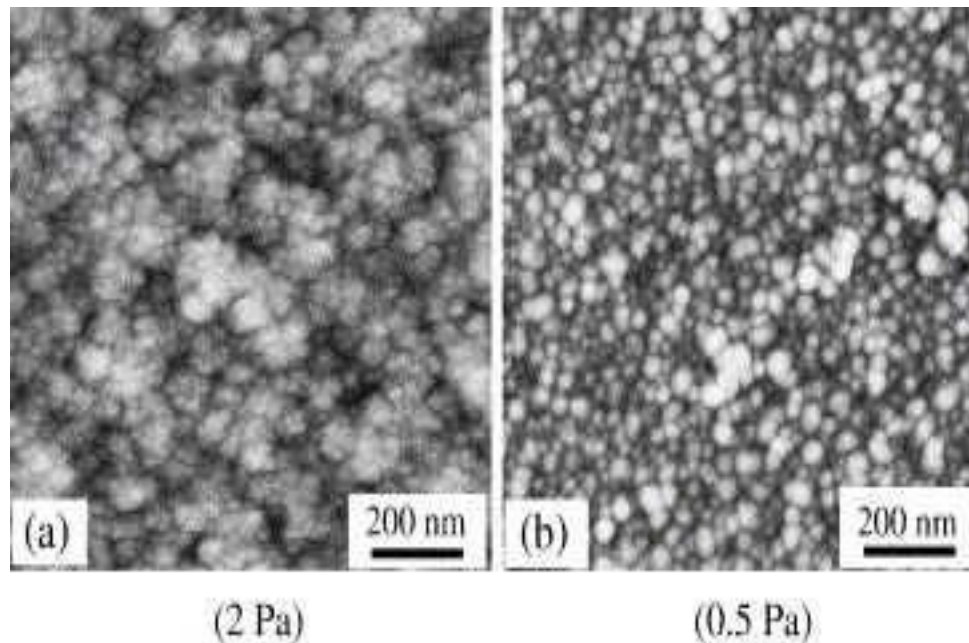
This bombardment of the layer by energetic species generates a compressive stress (see Fig. 3) in the planes parallel to the surface ( $a//$ ) and thus, an expansion in the planes normal to the surface ( $a$ ). In this way, the lattice parameter normal to the surface ( $a$ ) is increased, which explains the shift observed on the X-ray diagram (Fig. 2).

**Fig. 3. Effect of the stress on the lattice parameter ( $a_0$  = lattice parameter of the unstressed structure,  $a$  = lattice parameter normal to the surface,  $a_{//}$  = lattice parameter parallel to the surface)**



Observations by AFM (see Fig. 4) show the difference of morphology between porous layer (Fig. 4a) and dense layer (Fig. 4b). In the first case, the manifest porosity is located between grains; in the second case this one is much less perceptible. The grains size increased from 10–25 nm for porous layer to 20–50 nm for dense layer (i.e., when the argon pressure was decreased). Moreover, the film deposited at 0.5 Pa had a smoother surface ( $R_a = 1.9$  nm) than that deposited at 2 Pa ( $R_a = 2.9$  nm). This difference in the surface roughness is due to a variation in the distribution of incident angles and energy of the depositing atoms between low and high deposition pressures [27] and [28].

**Fig. 4. AFM images for cobalt–manganese–ferrite thin films deposited at 2 Pa (a) and 0.5 Pa (b) pressure**



Specific surface area of these samples was computed from adsorption isotherm (77 K) using the B.E.T. (Brunauer–Emmett–Teller) method [29]. Using krypton as the adsorptive gas, the B.E.T. surface area (SB.E.T.) is deduced from the monolayer volume [30] according to the relation

$$SB.E.T.=5.64\times 10^4 V_m.$$

Fig. 5 shows the change in surface for the thin films deposited at 2 Pa. For each measurement, samples were pre-heated at different temperatures (from 150 to 400 °C) during 16 h in order to degas the active surface. The SEF term (surface enhancement factor) used in the plot (Fig. 5) corresponds to the ratio between the measured surface area SB.E.T. to the nominal area  $S_0$  (projected area) of thin films. We can notice that the samples pre-heated at temperatures lower than 250 °C are not enough degassed. The maximum value (about 100 m<sup>2</sup>/m<sup>2</sup> of substrate) was obtained after an outgassing at 300 °C. This is equivalent to a specific surface area of 76 m<sup>2</sup>/g, if we take into account the amount of ferrite layer deposited on the substrate. By opposition, the SEF value measured for dense layer (deposited at 0.5 Pa) is only 2 m<sup>2</sup>/m<sup>2</sup> of substrate, which is in agreement with the results obtained by S. Capdeville [25] (see Table 3).

Thin films deposited at 0.5 Pa are much denser than those deposited at 2 Pa. The surface area that can participate in exchanges between the thin layer and the atmosphere is much greater for samples deposited at 2 Pa due to intergranular porosity. It should be also noted in Fig. 5 that at 400 °C, the SEF decreasing is due to a modification of the microstructure of the layer. Indeed, a comparison between the microstructure of porous thin layer before and after B.E.T. measurements highlights a growth of grains, which causes a decrease of active surface.

**Fig. 5. B.E.T. measurements of cobalt–Zinc–ferrite porous thin film pre-heated at various temperatures during 16 h.**

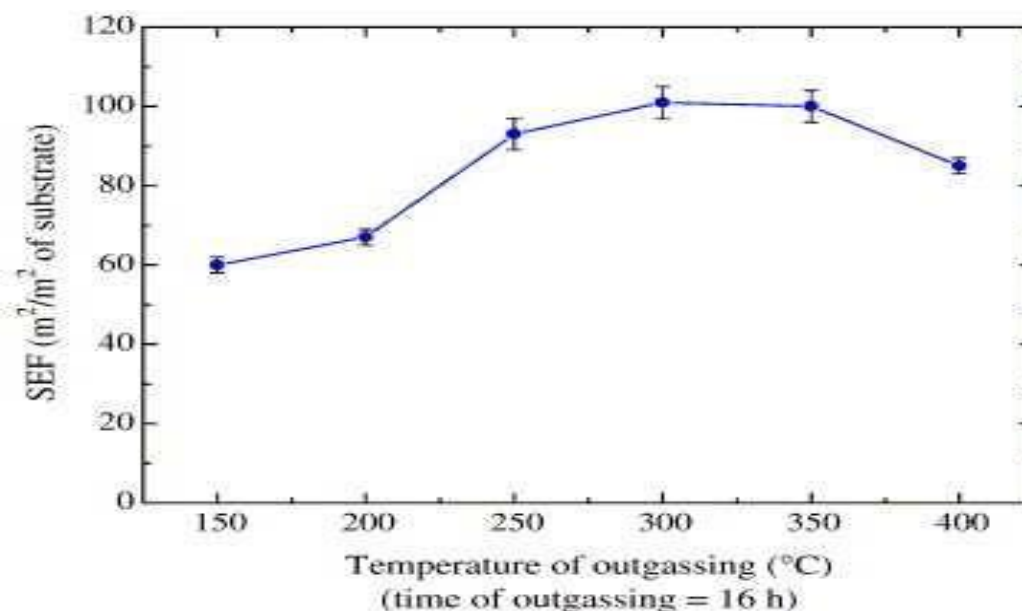


**Table3.**

**B.E.T .measurements results**

Sputtering conditions	Without magnetron		Without magnetron	Magnetron configuration
P <sub>Ar</sub> (Pa)	0.5	2	0.5	2
D(mm)	80	80	90	90
SEF(m <sup>2</sup> /m <sup>2</sup> of substrate)	2	35	2	100
References	[25]		Thiswork	

PA<sub>r</sub>=gas pressure (Pa); D=target-substrate distance (mm); SEF=surface enhancement factor (m<sup>2</sup>/m<sup>2</sup> of substrate). These results, which confirm previous AFM observations, are promising for a possible application of nanostructured substitute ferrite films as gas sensors.

## 4. Conclusions

We have shown in this work that cobalt–Zinc–ferrite thin films appear to be quite suitable for an application as gas sensors. The necessary properties are a low density and a high surface area, which implies a small crystallite size. The RF-sputtering method allows to obtain nanostructured and porous layers, by optimizing the deposition parameters. These results were confirmed by structural and microstructural characterizations (G-XRD and AFM). B.E.T. method, applied to the thin films, enabled us to make the link between the microstructure of thin layers and their surface area.



## References

1. N. Yamazoe, *Sens. Actuators, B, Chem.* 5 (1991), p. 7.
2. W. Gopel and D. Schierbaum, *Sens. Actuators, B, Chem.* 26 (1995) (1–3), p. 1.
3. G. Behr and W. Fhegel, *Sens. Actuators, B, Chem.* 33–37 (1995), p. 2627.
4. C.H. Kwon, H.-K. Hong, D.H. Yun, K. Lee, S.-T. Kim, Y.-H. Roh and B.-H. Lee, *Sens. Actuators, B, Chem.* 24–25 (1995), p. 610.
5. G. Magamma, V. Jayaraman, T. Gnanasekaran and G. Periaswami, *Sens. Actuators, B, Chem.* 53 (1998), p. 133.
6. Y. Yamada, Y. Seno, Y. Masuoka and K. Yamashita, *Sens. Actuators, B, Chem.* 49 (1998), p. 248.
7. Z. Jiao, S. Wang, L. Bian and J. Liu, *Mater. Res. Bull.* 35 (2000), p. 741.
8. N. Barsan, M. Schweizer-Berberich and W. Göpel, *Fresenius' J. Anal. Chem.* 365 (1999), p. 287.
9. T. Seiyama, H. Futata, F. Era and N. Yamazoe, *Mater. Sci.* 8 (1972), p. 63.
10. J. Xu, Y. Shun, Q. Pan and J. Qin, *Sens. Actuators, B, Chem.* 66 (2000), p. 161.
11. K. Zakrzewska, M. Radecka and M. Rekas, *Thin Solid Films* 310 (1997), p. 161.
12. K. Zakrzewska, *Thin Solid Films* 391 (2001), p. 229.
13. R.J. Rennard and W.L. Kehl, *J. Catal.* 21 (1971), p. 282.
14. Y. Zhihao and Z. Lide, *Mater. Res. Bull.* 33 (1998), p. 1587.
15. G.R. Dube and V.S. Darshane, *J. Mol. Catal.* 79 (1993), p. 285.
16. N.-S. Chen, X.-J. Yang, E.-S. Liu and J.-L. Huang, *Sens. Actuators, B, Chem.* 66 (2000), p. 178.
17. C.V. Gopal Reddy, S.V. Manorama and V.J. Rao, *Sens. Actuators, B, Chem.* 55 (1999), p. 90.
18. S. Tao, F. Gao, X. Liu and O.T. Sørensen, *Mater. Sci. Eng., B, Solid-State Mater. Adv. Technol.* 77 (2000), p. 172.
19. X. Niu, W. Du and W. Du, *Sens. Actuators, B, Chem.* 99 (2004), p. 405.
20. K. Ishizaka, Y. Kinemuchi, T. Suzuki, H. Suematsu, W. Jiang and K. Yatsui In: A. Kumar, Y.-W. Chung, J.J. Moore, G.L. Doll, K. Yasui and D.S. Misra, Editors, *TMS (The Minerals, Metals and Materials Society)* (2002), p. 79.
21. K. Madhusudan Reddy, L. Satyanarayana, S.V. Manorama and R.D.K. Misra, *Mater. Res. Bull.* 39 (2004), p. 1491.
22. Z. Jiao, M. Wu, J. Gu and Z. Qin, *IEEE Sens. J.* 3 (2003), p. 435.
23. C.-Y. Oh, J.-H. Oh and T. Ko, *IEEE Trans. Magn.* 38 (2002), p. 3018.
24. Q. Yan, R.J. Gambino, S. Sampath, L.H. Lewis, L. Li, E. Baumberger, A. Vaidya and H. Xiong, *Acta Mater.* 52 (2004), p. 3347.
25. S. Capdeville, P. Alphonse, C. Bonningue, L. Presmanes and P. Tailhades, *J. Appl. Phys.* 96 (2004), p. 6142.
26. H. Osada, K. Seki, H. Matsuki, S. Kikuchi and K. Murakami, *IEEE Trans. Magn.* 31 (1995), p. 3164.
26. Y. Hoshi, E. Suzuki and H. Shimizu, *Electrochim. Acta* 44 (1999), p. 3945.
27. T.J. Vink, W. Walrave, J.L.C. Daams, A.G. Dirks, M.A.J. Somers and K.J.A. van der Aker, *J. Appl. Phys.* 74 (1993), p. 988.
28. S. Brunauer, P.H. Hemmett and E. Teller, *J. Am. Chem. Soc.* 60 (1938), p. 309.
29. P.A. Webb and C. Orr, *Analytical Methods in Fine Particle Technology*, Micromeritics Instrument Corp., Norcross (1997).